Power Flow and Stability Analyses of a Multifunctional Distributed Generation System Integrating a Photovoltaic System With Unified Power Quality Conditioner

Leonardo Bruno Garcia Campanhol, Sérgio Augusto Oliveira da Silva, *Member, IEEE*, Azauri Albano de Oliveira, and Vinícius Dário Bacon

***Abstract*—This paper presents detailed studies involving sizing, stability analysis, and power flow through the series and parallel power converters in a multifunctional three-phase distributed generation (DG) system composed of a single-stage photovoltaic (PV) system integrated into a unified power quality conditioner (UPQC). The UPQC operates as a bidirectional interface when the DG system is placed between the grid and either generic loads or ac microgrid. In the grid-connected mode, the DG system performs active power-line conditioning, while injecting the energy produced by the PV array into the grid. In islanded operation, the system can act as ac grid forming via a parallel inverter, whether there is the presence of an energy storage system. A complete study involving the power flow through the PV-UPQC is mandatory to achieve the overall understanding of the system operation and designing the power converters properly. For this purpose, sizing curves are presented and discussed. Furthermore, two strategies aimed at limiting and/or decreasing the power processed by the series and parallel inverters are presented and discussed in detail. Both simulation and experimental results are presented to evaluate the static and dynamic performances of the PV-UPQC system operating grid connected and grid islanded.**

***Index Terms*—Distributed generation (DG) system, integrated photovoltaic (PV)-unified power quality conditioner (UPQC) system, power flow, stability analysis.**

I. Introduction

DISTRIBUTED generation (DG) systems based on renewable energy sources (RES) are currently emerging as an alternative for large and decentralized conventional power plants connected to long power transmission/distribution networks

Manuscript received March 27, 2018; revised June 18, 2018; accepted September 18, 2018. Date of publication September 30, 2018; date of current version May 2, 2019. Recommended for publication by Associate Editor S. Mekhilef. *(Corresponding author: Sérgio Augusto Oliveira da Silva.)*

L. B. G. Campanhol and V. D. Bacon are with the Electrical Engineering Department, Federal University of Technology, Apucarana, PR 86812-460, Brazil (e-mail:

which are related to the following indexes [20]: line utilization factor [power factor (PF) and fundamental PF], harmonic pollution factor, and load unbalance factor.

In [14]–[17], PV systems have acted similarly as parallel active power filters (P-APF), compensating for reactive power, as well as suppressing current harmonics generated by nonlinear loads. In [21]–[24], PV systems have been employed to operate integrated with unified power quality conditioners (UPQC) [25]–[28].

Although the main role of UPQC systems is performing series–parallel compensation, so that they can simultaneously act as series APF, compensating for mains voltages, as well as acting as P-APF, compensating the load currents, in [21] experimental results of the single-stage PV system integrated with UPQC performs only the function of a dynamic voltage restorer. In this case, only the disturbances of the grid voltages are compensated. In [22], a double-stage PV system integrated with the UPQC, named SPV-UPQC-P, has been evaluated only through computer simulations. However, this system only compensates reactive power of the load and unbalances of the grid voltage. Thus, the suppression of grid voltage as well as load current harmonics has not been taken into account. Another application in which the PV system is integrated with the UPQC is presented in [23]. In this application, the system can operate as a grid forming in an ac microgrid [19], since different types of DG sources (PV, wind, and others), as well as energy storage systems, can be used as grid-forming units in an islanded microgrid [29]. However, transients/disturbances could be observed in the voltages that fed the load when the system was transferred from the grid-connected operation mode to the grid-islanded operation mode. This happens because the parallel converter of the UPQC needs to change its control mode from current source to voltage source. The same effect occurs when the system returns to operate in the grid-connected mode, because the parallel converter must be controlled again as the current source.

In [24], the system called the PV-UPQC has been presented. It can operate in both three-phase three-wire and three-phase four-wire EPS. Since the parallel converter is voltage controlled, so that balanced and regulated voltages can be provided to the load, there is no need to change its control mode when the system operates as grid forming in an ac microgrid. In other words, the parallel converter is voltage controlled in both grid-connected and grid-islanded modes. On the other hand, the mentioned system can also operate either as grid feeding or grid supporting [19] in an ac microgrid, since the control mode of the parallel converter can also be switched to operate from voltage source to current source.

On the other hand, in [24], studies related to stability analysis, detailed study related to active and apparent power flows and mainly the sizing and protection of the power converters that compose the PV-UPQC system, have not been addressed. Thereby, additional research advances and contributions are presented in this paper, as follows.

1) A complete study involving the power flow through the PV-UPQC system for obtaining the overall understanding of the system working under several operation modes is performed. This study represents an important and useful methodological tool for designing the power converters properly. It is supported by means of an extensive number of sizing curves and allows the designer an effective power converters sizing.
2) A strategy to avoid over power rating of the series and parallel power converters is implemented. This strategy is needed in order to establish the priority of the power flow through the converters, since the PV-UPQC system performs, simultaneously, grid active power injection (energy produced from the PV system), as well as the power-line conditioning.
3) The stability analysis of the PV system is performed. In the context of a UPQC, the study involving the ability of the series and parallel converters to remain stable even in the occurrence of disturbances in both the load currents and grid voltages has never been addressed before in the literature and appears as an important and necessary subject to be discussed. Furthermore, it is checked if the system stability is affected or not by different grid impedance characteristics.
4) The PV-UPQC system is also tested in grid-islanded operation. This operation mode allows exploring new aspects related to the multifunctionality of the PV-UPQC system.

This paper is organized as follows. Section II contains the description of the PV-UPQC system, as well as the strategies used to control the series and parallel inverters in grid-connected and grid-islanded operation modes. Section III contains detailed descriptions of the active and apparent power flows through the PV-UPQC resulting normalized curves for a proper sizing of the series and parallel neutral point clamped (NPC) inverters. In addition, power limitation strategies applied to the power converters are presented. Section IV contains the descriptions of system stability analysis, while in Section V, the strategy developed to avoid the over power rating of the parallel NPC inverter is tested. In Section VI, both static and dynamic performances of the system are evaluated according to the experimental results. Finally, Section VII presents the conclusions.

II. Description of the PV-UPQC System

Fig. 1 shows the power circuit of the three-phase single-stage PV-UPQC system. The series and parallel converters consist of three-level NPC inverters. The series inverter is connected to the grid by means of three coupling transformers connected in series with *L* filters, represented by the inductances L_{sc_abc} in series with their respective internal resistances R_{sc_abc}. The parallel inverter is connected to the point of common coupling 2 (PCC_2) through *LC* filters represented by the inductances L_{pc_abc} in series with their respective internal resistances R_{pc_abc}, in addition the capacitances C_{p_abc}. The dc bus is composed of the capacitors C_{dc1} and C_{dc2} connected in parallel with the PV array consisting of a string with 20 series-connected PV panels.

The operating voltage of the PV system is determined by the MPPT algorithm called perturb and observe (P&O) [16]. Thus, the maximum amplitude of the dc-bus voltage ($v^{*}_{\mathrm{dc\_max}}$) is around 600 V, allowing the PV system to operate in MPP at standard test conditions (STC). On the other hand, the minimum

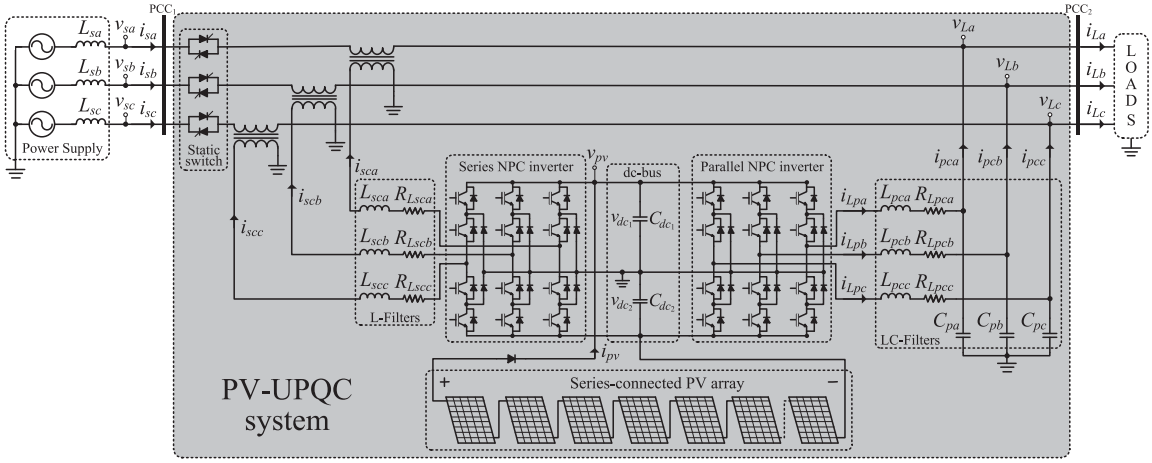

Fig. 1. Power circuit structure of the PV-UPQC system.

system operation voltage $(v^*_{\mathrm{dc\_min}})$ is set at 460 V, i.e., the PV system operates outside the MPP when this voltage is reached. In adverse situations, i.e., when the PV is under maintenance or at night, the PV-UPQC system operates as a conventional UPQC. In this situation, the minimum dc-bus voltage is also set at 460 V.

A. Control Strategy of the PV-UPQC System

The input currents of the PV-UPQC system are controlled to be synchronized with grid voltages. These currents are controlled by a series converter, so that the series converter behaves like a balanced sinusoidal current source. Consequently, a high impedance path for the load harmonic currents is created between grid and load, meaning that the series converter behaves like a harmonic isolator. Since the grid currents are sinusoidal and in phase with the grid voltages, there is no flow of reactive power and harmonics in the grid (PCC_1). Thus, a high PF is obtained in addition to the compensation of load unbalance. The dc-bus voltage controller adjusts the amplitude of grid currents, so that the power flow balance involving the grid, the PV system, and the load is reached. Moreover, the compensated grid currents can be in phase or in phase opposition with the grid voltages, as discussed in detail in the next section.

The output voltages of the PV-UPQC system are also controlled to be synchronized and in phase with the grid voltages. The respective voltages are controlled by a parallel converter, i.e., the parallel converter behaves like a voltage sinusoidal source. Thus, a low impedance path for the load harmonic currents is created to facilitate the flow of these currents through the parallel converter. Since the system output voltages are controlled to be sinusoidal, balanced, and regulated, any disturbance present in the grid, such as voltage harmonics, voltage unbalances, and voltage sags/swells will appear across the terminals of the series coupling transformers.

The compensation strategy used in the PV-UPQC system is known as a dual compensation strategy and it is described in detail in [25]–[27], where are discussed the advantages over conventional compensation strategies [28] used to control most UPQCs presented in the literature.

In this paper, the algorithms used to generate the references of the grid currents (series NPC inverter), output voltages (parallel NPC inverter), and dc-bus voltage (MPPT-P&O) are implemented in the synchronous reference frame (SRF), as shown in Fig. 4(a) and (b). These respective algorithms, the mathematical modeling of converters, the voltage controllers (parallel inverter and dc bus), as well as the current controllers (series inverter), are presented in detail in [24]. The phase-locked loop scheme, which is used for the synchronization and the utility phase-angle detection, is presented in [30].

B. Operating Modes of the PV-UPQC System

The multifunctionality of the PV-UPQC system can be highlighted by its number of operating modes (OPMs), described as follows.

1) *OPM 1:* In OPM 1, the PV-UPQC system is connected to the grid without the connected load. In this case, all the power generated by the PV system is injected into the grid (operating as a conventional DG system).
2) *OPM 2:* In OPM 2, the PV-UPQC system is connected to the grid with the connected load and without power generation from the PV array. In this case, the system only performs power-line conditioning since it operates as a conventional UPQC (grid-supporting [19]).
3) *OPM 3:* In OPM 3, the PV-UPQC system is connected to the power grid with both load and power generation from the PV array. In this case, the system performs power-line conditioning and supplies power to the grid/load. If the power generated by the PV system is greater than the energy demanded by the load, the energy surplus is injected into the grid. If it is lower, all the generated energy is sent to the load (grid feeding and grid supporting [19]).
4) *OPM 4:* In OPM 4, the PV-UPQC system is disconnected from the grid (islanded operation mode) with both the load connected to the PCC_2 (see Fig. 1) and the power generation by the PV array. In this case, the operation of the series converter is inhibited and the load is fed by the power produced from the PV array through the voltage-controlled parallel converter. For a given application, the

system can act as a grid forming [19], provided that a storage energy system being present.

5) *OPM 5:* In OPM 5, the PV-UPQC system is disconnected from the grid (islanded operation mode) with both the load connected to the PCC_2 and the power generation by the PV array. In this case, operation of the series converter is inhibited and the load is fed by the current-controlled parallel converter (grid feeding [19]). This operation mode is not addressed in this paper.

III. Power Flow Through the PV-UPQC System

This section presents the quantitative study involving power flows through the series and parallel converters of the PV-UPQC system. For purposes of analysis, the following conditions are assumed for the system operating in the steady state: 1) grid voltages are balanced although they may contain harmonics; and 2) currents drained from the grid are balanced and sinusoidal. Based on the mentioned conditions, the entire study is conducted representing the PV-UPQC system through an equivalent single-phase system.

Beyond allowing a clear understanding of the system functioning, this study intends to offer subsidies for the realization of an adequate sizing of the series and parallel power converters. Such subsidies are provided by means of curves, in which the apparent powers of both converters are normalized in function of the total apparent power of the load.

In particular, the apparent powers involved in the power flow through the series and parallel NPC inverters depend on the characteristics of the utility grid, the load, as well as the energy produced by the PV array. These characteristics are described as follows.

1) Ratio between the grid and load rms voltages (V_s/V_L).
2) Total harmonic distortion of the grid voltages (THD_{V_s}) and load currents (THD_{i_L}).
3) Fundamental PF of the load (PF_{1L}).
4) Active power absorbed by the dc bus ($P_{\text{B dc}}$) for compensation of the system losses, i.e., the losses in switching elements and passive filtering elements.
5) Active power produced by the PV array (P_{pv}).

A. Apparent Power of the Series NPC Inverter

The complex apparent power of the series NPC inverter ($\dot{S}_{sc}$) is given by

$$\dot{S}_{sc} = \dot{V}_{Tsc}\dot{I}_s^* \tag{1}$$

where $\dot{V}_{Tsc} = \dot{V}_s - \dot{V}_L$ is the rms complex voltage on the series coupling transformer; $\dot{V}_s$ and $\dot{V}_L$ are the rms complex voltages in the grid and load, respectively; and $\dot{I}_s^*$ is the complex conjugate of the rms grid current.

In the steady state, both the grid currents (i_{s_abc}) and load voltages (v_{L_abc}) are controlled to be sinusoidal and in phase with the fundamental positive-sequence components of the grid voltages (v_{s_abc}), since they can be unbalanced and contain harmonics. Under ideal conditions, it is assumed that both i_{s_abc} and v_{L_abc} have only fundamental components. Furthermore, the rms value of the grid voltage V_s is assumed to be composed of fundamental and harmonic components represented by V_{s1} and V_{sH}, respectively. Thereby, complex power modulus (apparent power) of the series converter is given by

$$|S_{sc}| = \sqrt{\left[\left(V_{s1} - V_L\right) I_s\right]^2 + \left(V_{sH} I_s\right)^2}. \tag{2}$$

The term ($V_{sH} I_s$) in (2) represents the voltage distortion power (D_{V_s}), which is defined in [20] by

$$D_{V_s} = V_{sH} I_s = S_{s1}\text{THD}_{V_s} \tag{3}$$

where $S_{s1} = V_{s1} I_s$ is the apparent fundamental power of the grid.

By replacing (3) in (2) and after some mathematical manipulations, $|S_{sc}|$ can be obtained as follows:

$$|S_{sc}| = \sqrt{\left[V_{s1} I_s \left(1 - V_L/V_{s1}\right)\right]^2 + \left(S_{s1}\text{THD}_{V_s}\right)^2}. \tag{4}$$

Considering that all the fundamental apparent power drained from the grid is equal to the active power demanded by the load (P_L), i.e., $S_{s1} = P_L$, (4) can be rewritten as

$$|S_{sc}| = \sqrt{P_L^2 \left[\left(1 - V_L/V_{s1}\right)^2 + \text{THD}_{V_s}^2\right]}. \tag{5}$$

Assuming the load voltages sinusoidal and balanced, the complex power modulus of the load ($|S_L|$) is obtained by

$$|S_L| = \sqrt{P_L^2 + Q_L^2 + D_L^2} \tag{6}$$

where Q_L and D_L are the reactive and harmonic powers of the load, respectively.

By normalizing $|S_{sc}|$ according to $|S_L|$ results in

$$\frac{|S_{sc}|}{|S_L|} = \frac{\sqrt{P_L^2 \left[\left(1 - V_L/V_{s1}\right)^2 + \text{THD}_{V_s}^2\right]}}{\sqrt{P_L^2 + Q_L^2 + D_L^2}}. \tag{7}$$

Considering the assumption mentioned above, the total load power factor (PF_L) can be written as

$$PF_L = \frac{P_L}{S_L} = \frac{PF_{1L}}{\sqrt{1 + \text{THD}_{i_L}^2}}. \tag{8}$$

By replacing (8) in (7) and after some mathematical manipulations, $|S_{sc}|/|S_L|$ can be obtained as follows:

$$\frac{|S_{sc}|}{|S_L|} = \frac{PF_{1L}\sqrt{\left(1 - \frac{V_L}{V_{s1}}\right)^2 + \text{THD}_{V_s}^2}}{\sqrt{1 + \text{THD}_{i_L}^2}}. \tag{9}$$

The complex power modulus S_{sc} can also be calculated including the active power consumed by the dc bus ($P_{B\text{dc}}$), as well as the active power (P_{pv}) produced by the PV array. Thus, the fundamental apparent power of the grid is calculated by

$$S_{s1} = P_T = P_L + \left(P_{B\text{dc}} - P_{\text{pv}}\right)/3 = P_L\left(1 + k_{B\text{dc}} - k_{\text{pv}}\right) \tag{10}$$

where P_T is the total active power of the grid, while the terms $k_{B\text{dc}}$ and k_{pv} represent the respective ratios involving $P_{B\text{dc}}$ and

$P_{\rm pv}$ in relation to P_L, as follows:

$$k_{B\rm dc} = \frac{P_{B\rm dc}}{3P_L} \tag{11}$$

$$k_{pv} = \frac{P_{pv}}{3P_L}. \tag{12}$$

Thereby, by substituting (10)–(12) into (4), $|S_{sc}|/|S_L|$ is obtained as follows:

$$\frac{|S_{sc}|}{|S_L|} = \frac{\mathrm{PF}_{1L}\sqrt{(1+k_{B\rm dc}-k_{\rm pv})^2\left[\left(1-\frac{V_L}{V_{s1}}\right)^2+\mathrm{THD}_{V_s}^2\right]}}{\sqrt{1+\mathrm{THD}_{i_L}^2}}. \tag{13}$$

B. Apparent Power of the Parallel NPC Inverter

The complex apparent power of the parallel NPC inverter ($\dot{S}_{pc}$) is given by

$$\dot{S}_{pc} = \dot{S}_L - \dot{V}_L \dot{I}_s^* \tag{14}$$

where $\dot{S}_L$ is the complex apparent power of the load.

Supposing that the grid currents (i_{s_abc}) are sinusoidal and in phase with the respective grid voltages v_{s_abc}, and assuming that $S_{s1} = P_L$, the complex power modulus (apparent power) of the parallel NPC inverter ($|S_{pc}|$) can be calculated by

$$|S_{pc}| = \sqrt{P_L^2 + Q_L^2 + D_L^2} - P_L\left(V_L/V_{s1}\right). \tag{15}$$

By rearranging (15), results in

$$|S_{pc}| = \sqrt{\left[P_L\left(1-V_L/V_{s1}\right)\right]^2 + Q_L^2 + D_L^2}. \tag{16}$$

After some mathematical manipulating in (16) and considering S_L can be obtained from (8), $|S_{pc}|$ is found as

$$|S_{pc}| = \sqrt{P_L^2\left[\left(\frac{V_L}{V_{s1}}\right)^2 - 2\left(\frac{V_L}{V_{s1}}\right) + \frac{1+\mathrm{THD}_{i_L}^2}{PF_{1L}^2}\right]}. \tag{17}$$

By normalizing $|S_{pc}|$ according to $|S_L|$, $|S_{pc}|/|S_L|$ can be obtained as

$$\frac{|S_{pc}|}{|S_L|} = \sqrt{\frac{PF_{1L}^2\frac{V_L}{V_{s1}}\left(\frac{V_L}{V_{s1}}-2\right)}{1+\mathrm{THD}_{i_L}^2}+1}. \tag{18}$$

By including the active power $P_{B\rm dc}$ and $P_{\rm pv}$ into the analysis, (18) can be rewritten as

$$\frac{|S_{pc}|}{|S_L|} = \sqrt{\frac{\mathrm{PF}_{1L}^2\frac{V_L}{V_{s1}}\left(1+k_{B\rm dc}-k_{\rm pv}\right)\left[\frac{V_L}{V_{s1}}\left(1+k_{B\rm dc}-k_{\rm pv}\right)-2\right]}{1+\mathrm{THD}_{i_L}^2}+1}. \tag{19}$$

C. Apparent Power Normalized Curves of the PV-UPQC System

Fig. 2 shows the curves of the apparent powers of series and parallel converters, normalized based on total apparent power of the load, i.e., $|S_{sc}|/|S_L|$ and $|S_{pc}|/|S_L|$, respectively.

In Fig. 2(a) and (b), the apparent power normalized curves, considering the factors $k_{B\rm dc} = 0$ and $k_{\rm pv} = 0$, are shown. According to Fig. 2(a), when $\mathrm{THD}_{V_s} = 0$, the series converter only processes power when the ratio $V_s/V_L \neq 1$. When $\mathrm{THD}_{V_s} > 0$, however, the processed power increases in the entire range covering the ratio V_s/V_L, i.e., $0.75 < V_s/V_L < 1.25$. In Fig. 2(b), according to the curve $|S_{pc}|/|S_L|$, the higher the THD_{iL} and the lower the PF_{1L}, the greater the power handled by the parallel converter. Fig. 2(c) and (d) shows the normalized curves considering $k_{B\rm dc} = 0.1$ and $k_{\rm pv} = 0$, respectively. In this case, active power is assumed being drained from the grid to regulate the dc-bus voltage to maintain the power balance of the system. Therefore, the power processed by the series converter increases when $V_s/V_L \neq 1$ or $\mathrm{THD}_{V_s} > 0$, as shown in Fig. 2(c). In addition, at certain points of the curves $|S_{pc}|/|S_L|$ shown in Fig. 2(d), an increase in the power processed by the parallel converter can also be observed, as, for example, under the condition in which $V_s/V_L = 1$, $\mathrm{THD}_{iL} = 0\%$, and $\mathrm{PF}_{1L} = 1$. On the other hand, depending on the ratio V_s/V_L, the mentioned active power can be processed by any one of the converters (series or parallel) or simultaneously by both.

For the condition where $k_{B\rm dc} = 0$ and $k_{\rm pv} = 0.1$, when $V_s/V_L \neq 1$ or $\mathrm{THD}_{V_s} > 0$, the power processed by the series converter decreases, as shown in Fig. 2(e). This occurs because part of the active power of the load is provided by the PV array, reducing the power drained from the grid. Thus, depending on the value of V_s/V_L, the parallel converter processes all the active power drained from the PV array, as shown in Fig. 2(f).

Fig. 2(g) and (h) shows the normalized power curves considering $k_{B\rm dc} = 0$ and $k_{\rm pv} = 0.5$. In this case, 50% of the total active power consumed by the load is provided by the PV array. Thus, according to the curves shown in Fig. 2(g), it is verified that the lower the power drained from the grid, the lower the power processed by the series converter. Since all or most of the active power generated by the PV array flows through the parallel converter, Fig. 2(h) shows an increase in the power processed by the referred converter for this operating condition.

Fig. 2(i) and (j) shows the power curves for $k_{\rm pv} = 1.5$, for the condition in which $P_{\rm pv} > P_L$. In this case, the active power injected into the grid equals 50% of the active power consumed by the load. Comparing the curves in Fig. 2(g) and (i), in both cases, regardless of the power flow direction, the series converter processes the same amount of power. According to the curves in Fig. 2(j), however, depending on the ratio V_s/V_L, the parallel converter processes all the active power generated by the PV array. Moreover, part of this energy is provided to the load and the remaining is injected into the grid.

D. Active Power Flow Through the PV-UPQC System

Fig. 3 shows the instantaneous active power flow through the converters that compose the PV-UPQC system. The directions of power flow are influenced by the following features: 1) amount of energy produced by the PV array; 2) amount of energy consumed by the load; and 3) difference between grid (V_s) and load (V_L) rms voltages. The instantaneous active powers involved in the analysis are described as follows: power of the grid (p_s), power of the PV array ($p_{\rm pv}$), power of the series

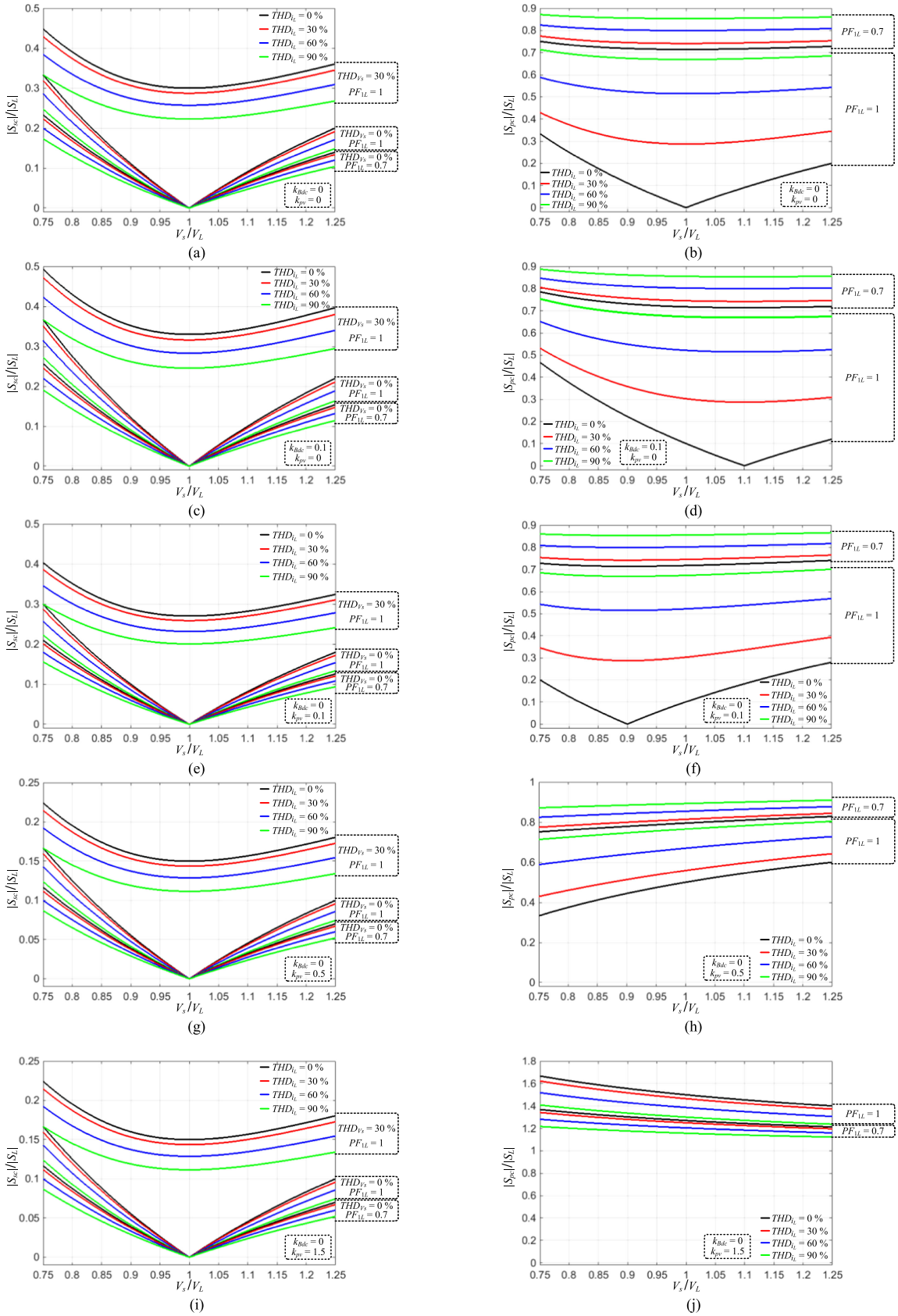

Fig. 2. Apparent power normalized curves of the series and parallel converters. (a) $|S_{sc}|/|S_L|$ for $k_{B\,\mathrm{dc}} = 0$ and $k_{\mathrm{pv}} = 0$. (b) $|S_{pc}|/|S_L|$ for $k_{B\,\mathrm{dc}} = 0$ and $k_{\mathrm{pv}} = 0$. (c) $|S_{sc}|/|S_L|$ for $k_{B\,\mathrm{dc}} = 0.1$ and $k_{\mathrm{pv}} = 0$. (d) $|S_{pc}|/|S_L|$ for $k_{B\,\mathrm{dc}} = 0.1$ and $k_{\mathrm{pv}} = 0$. (e) $|S_{sc}|/|S_L|$ for $k_{B\,\mathrm{dc}} = 0$ and $k_{\mathrm{pv}} = 0.1$. (f) $|S_{pc}|/|S_L|$ for $k_{B\,\mathrm{dc}} = 0$ and $k_{\mathrm{pv}} = 0.1$. (g) $|S_{sc}|/|S_L|$ for $k_{B\,\mathrm{dc}} = 0$ and $k_{\mathrm{pv}} = 0.5$. (h) $|S_{pc}|/|S_L|$ for $k_{B\,\mathrm{dc}} = 0$ and $k_{\mathrm{pv}} = 0.5$. (i) $|S_{sc}|/|S_L|$ for $k_{B\,\mathrm{dc}} = 0$ and $k_{\mathrm{pv}} = 1.5$. (j) $|S_{pc}|/|S_L|$ for $k_{B\,\mathrm{dc}} = 0$ and $k_{\mathrm{pv}} = 1.5$.

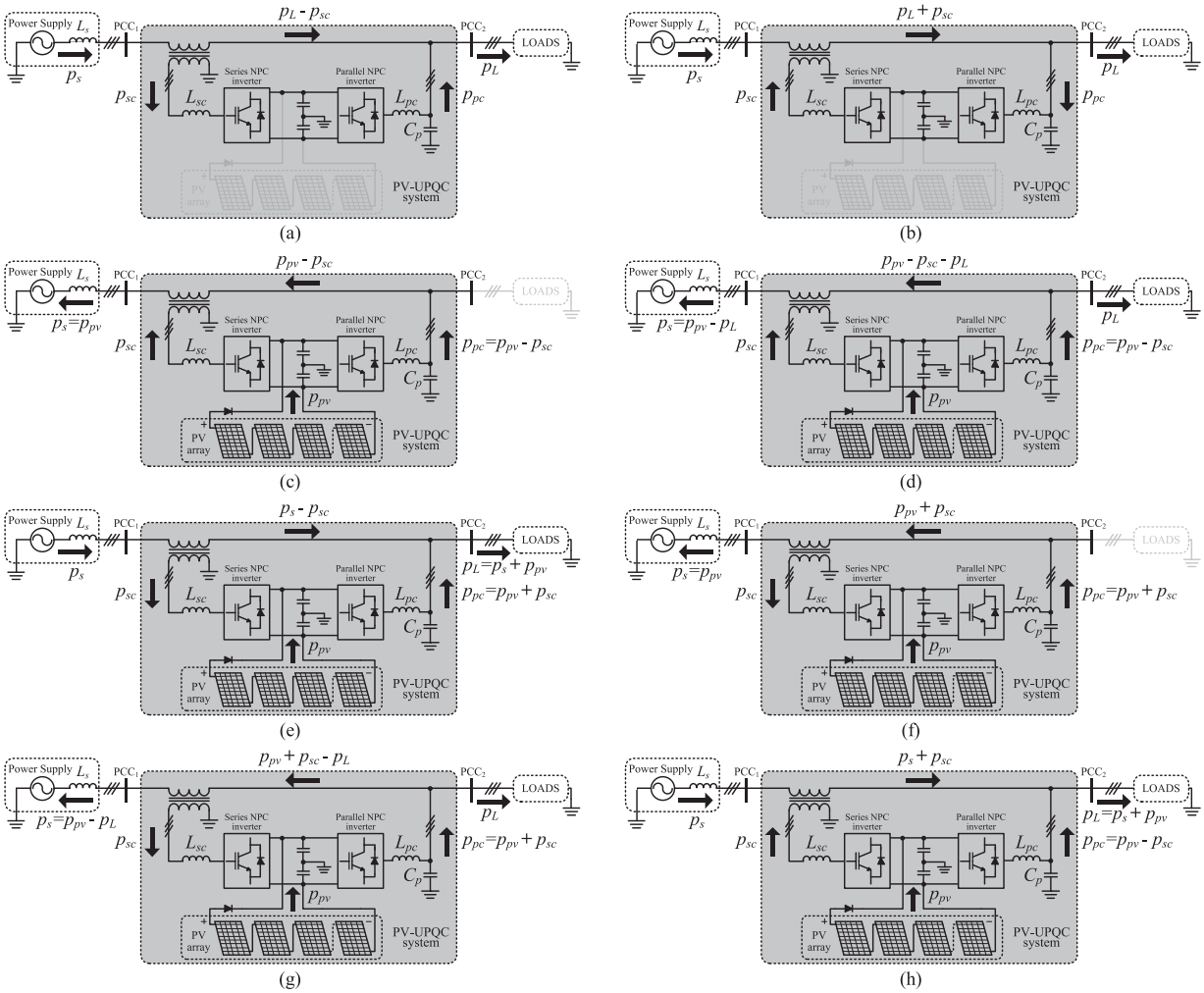

Fig. 3. Active power flow through the PV-UPQC system. (a) $V_s > V_L$ with $P_L \neq 0$ and $P_{\text{pv}} = 0$. (b) $V_s < V_L$ with $P_L \neq 0$ and $P_{\text{pv}} = 0$. (c) $V_s > V_L$ with $P_L = 0$ and $P_{\text{pv}} > 0$. (d) $V_s > V_L$ with $P_{\text{pv}} > P_L$. (e) $V_s > V_L$ with $P_{\text{pv}} < P_L$. (f) $V_s < V_L$ with $P_L = 0$ and $P_{\text{pv}} > 0$. (g) $V_s < V_L$ with $P_{\text{pv}} > P_L$. (h) $V_s < V_L$ with $P_{\text{pv}} < P_L$.

TABLE I
CONDITIONS ADOPTED TO DETERMINE THE ACTIVE POWER FLOW THROUGH THE PV-UPQC SYSTEM

Conditions	Voltages	Load Power	PV Power
1	$V_s > V_L$	$P_L \neq 0$	$P_{pv} = 0$
2	$V_s < V_L$	$P_L \neq 0$	$P_{pv} = 0$
3	$V_s > V_L$	$P_L = 0$	$P_{pv} > 0$
4	$V_s > V_L$	$P_L > 0$	$P_{pv} > P_L$
5	$V_s > V_L$	$P_L > 0$	$P_{pv} < P_L$
6	$V_s < V_L$	$P_L = 0$	$P_{pv} > 0$
7	$V_s < V_L$	$P_L > 0$	$P_{pv} > P_L$
8	$V_s < V_L$	$P_L > 0$	$P_{pv} < P_L$

converter (p_{sc}), power of the parallel converter (p_{pc}), and power of the load (p_L). In this analysis, the losses in the switching elements of the NPC inverters or in the passive elements of the PV-UPQC system are not included, i.e., the analysis considers $k_{B\text{dc}} = 0$.

Table I shows all the operating conditions used to determine the active power flow through the converters.

Fig. 3(a) and (b) shows the power flow through the PV-UPQC system for $P_{\text{pv}} = 0$ W. In this case, all the load active power is drained from the utility grid. In Fig. 3(a), when $V_s > V_L$, part of the power flows from the grid to the series inverter and from the parallel inverter to the load. On the other hand, when $V_s < V_L$, the direction of the power flow changes, as shown in Fig. 3(b). In Fig. 3(c)–(e), it is assumed that $V_s > V_L$ and $P_{\text{pv}} \neq 0$ W. It can be seen in Fig. 3(c) that, as $p_L = 0$ W, all the energy generated by the PV array is provided to the grid through both inverters. It is also noticed that most of this energy is always processed by the parallel converter. In Fig. 3(d), it is assumed that $p_L \neq 0$ W and $p_{\text{pv}} > p_L$. In this case, part of the energy generated by the PV array is provided to the grid by mean of the series and parallel inverters, while the energy remaining is sent to the load through the parallel inverter. In Fig. 3(e), it is considered that $p_L \neq 0$ W and $p_{\text{pv}} < p_L$. In this case, all the energy produced by the PV array is provided to the load via a parallel inverter, while the energy remaining is drained from the grid. It can be observed that part of the energy provided by the grid flows through both the series and parallel inverters.

In Fig. 3(f)–(h), it is assumed that $V_s < V_L$ and $p_{\text{pv}} \neq 0$ W. In Fig. 3(f), as $p_L = 0$ W, all the energy produced by the PV array is provided to the grid through the parallel inverter.

TABLE II
OPERATING CONDITIONS ADOPTED FOR SCALING SERIES AND PARALLEL NPC INVERTERS

Operating Conditions	THD_{Vs}	THD_{iL}	PF_{1L}	V_s/V_L	K_{Bdc}	k_{pv}	$\|S_L\|$ [VA]	$\|S_{sc}\|$ [VA]	$\|S_{sc}\|/\|S_L\|$	$\|S_{pc}\|$ [VA]	$\|S_{pc}\|/\|S_L\|$
1	0 %	0 %	1	1	0	2	500	0	0	1000	2
2	15 %	0 %	1	0.75	0	0	500	182.76	0.366	166.66	0.333
3	15 %	100 %	1	0.75	0	2	707.10	182.76	0.258	1269.30	1.795

In addition, the active power that flows through the series inverter also flows through the parallel inverter. In Fig. 3(g), it is assumed that $p_L \neq 0$ W and $p_{\text{pv}} > p_L$. In this case, part of the energy produced by the PV array is provided to the power grid through the parallel inverter, while the energy remaining is sent to the load. As can be noticed, there is also a flow of active power through the series inverter. In Fig. 3(h), it is considered that $p_L \neq 0$ W and $p_{\text{pv}} < p_L$. In this case, the energy generated by the PV array is sent to the load through both the series and parallel inverters, while the energy remaining is drained from the grid.

Ideally, when $V_s = V_L$, there is no active power flow through the series inverter, as can be seen by the curves shown in Fig. 2(a), (c), (e), (g), and (i).

E. Examples of Sizing of the Series and Parallel NPC Inverters

Based on the analysis of the power flow presented previously, in this section, some examples of sizing of the series and parallel converters are performed considering three conditions of operation of the PV-UPQC system. In such sizing, it is considered that the load is connected to the system and it consumes active power $P_L = 500$ W per phase. Under the first operating condition, an ideal case is assumed where $\text{THD}_{V_s} = 0\%$, $\text{THD}_{i_L} = 0\%$, $\text{PF}_{1L} = 1$, and $V_s/V_L = 1$. For this case, it is considered that the PV array connected to the dc bus has a maximum capacity of generation, such as twice the active power consumed by the load, so that $k_{\text{pv}} = 2$. Thus, it follows that $|S_L| = 500$ VA, $|S_{sc}| = 0$ VA, and $|S_{pc}| = 1000$ VA, which results in $|S_{sc}|/|S_L| = 0$ and $|S_{pc}|/|S_L| = 2$. Therefore, it is verified that all the active power drained from the PV array is processed by the parallel converter. Thus, the sizing of this converter should be carried out taking into account the maximum active power being provided by the PV array. Under the second operating condition, it is assumed that the grid voltages with high harmonic content ($\text{THD}_{V_s} = 15\%$), as well as the system, operate with a voltage sag of 25% ($V_s/V_L = 0.75$). In addition, considering $\text{THD}_{i_L} = 0\%$, $\text{PF}_{1L} = 1$, and $k_{\text{pv}} = 0$, results $|S_L| = 500$ VA, $|S_{sc}| = 182.76$ VA, and $|S_{pc}| = 166.66$ VA, so that $|S_{sc}|/|S_L| = 0.366$ and $|S_{pc}|/|S_L| = 0.333$. Thus, even considering the utility grid operating under voltage disturbances (sags/harmonics), the series converter can be sized for a power rating less than 40% of the load nominal power. Therefore, it is evident that the low power level processed by the series converter represents great advantage for the PV-UPQC system. On the other hand, it is verified that the parallel converter processes power even when $\text{THD}_{i_L} = 0\%$ and $\text{PF}_{1L} = 1$, since $V_s/V_L \neq 1$. However, voltage sag disturbances must be considered in the sizing of this converter. Under the third operating condition, it is assumed that the load currents have high harmonic contents, i.e., $\text{THD}_{i_L} = 100\%$. It is also assumed that $\text{THD}_{V_s} = 15\%$, $\text{PF}_{1L} = 1$, $V_s/V_L = 0.75$, and $k_{\text{pv}} = 2$. For this operating condition, $|S_L| = 707.10$ VA, $|S_{sc}| = 182.76$ VA, and $|S_{pc}| = 1269.30$ VA, which results in $|S_{sc}|/|S_L| = 0.258$ and $|S_{pc}|/|S_L| = 1.795$. Thus, comparing this operation condition with the other two presented above, it is seen that the power processed by the parallel converter increases, showing that the sizing of this converter should also consider the nonactive power consumed by the load.

Table II summarizes the values adopted for the sizing of series and parallel converters.

F. Power Limitation Strategies Applied to the Series and Parallel NPC Inverters

This section presents strategies that are used to optimize the power flow through the series and parallel converters. Once the maximum energy being processed by the NPC inverters has been defined, it is required to use some strategy to guarantee that no over power rating of the NPC inverters occurs. In other words, it is necessary to limit the inverters power processing up to their nominal power rating, so that they can be adequately protected even if the load energy demand is more than the nominal one.

1) Power Limitation to Protect the Parallel Converter: Fig. 4(a) shows the control loop of the series NPC inverter in which the proposed current reference generation strategy is included. It must be emphasized that the parallel NPC inverter is sized considering both the active energy produced by the PV array as well as the nonactive power consumed by the nonlinear load. However, if an unexpected increase in the nonlinear load power demand occurs, the power rating of the parallel NPC inverter can be exceeded. Thus, to overcome this undesired condition, the current references of the series current control loop must be adjusted to allow the power limitation capability of the parallel converter. As can be seen in the shaded areas shown in Fig. 4(a), the nonfundamental components of the load currents in *dq*0 axes (i_{Ldh}, i_{Lq}, and i_{L0}) are added to the series converter current references whenever the constant K_{pc}, defined in (20), is greater than zero ($0 < K_{pc} < 1$). In other words, it means that, when the parallel converter exceeds its nominal power rating, the additional nonfundamental load currents will be drained from the grid, keeping the parallel converter within its power rate range. The constant K_{pc} computation is given by

$$K_{pc} = 1 - \frac{I_{Lna_{\max}}}{I_{Lna}} = 1 - \frac{\sqrt{I_{pc}^2 - (I_{\text{pv}} + I_{B\text{dc}})^2}}{I_{Lna}} = 1 - \frac{\sqrt{I_{pc}^2 - \left[\frac{1}{\sqrt{3}}(i_{ff} - i_{\text{dc}})\right]^2}}{I_{Lna}} \tag{20}$$

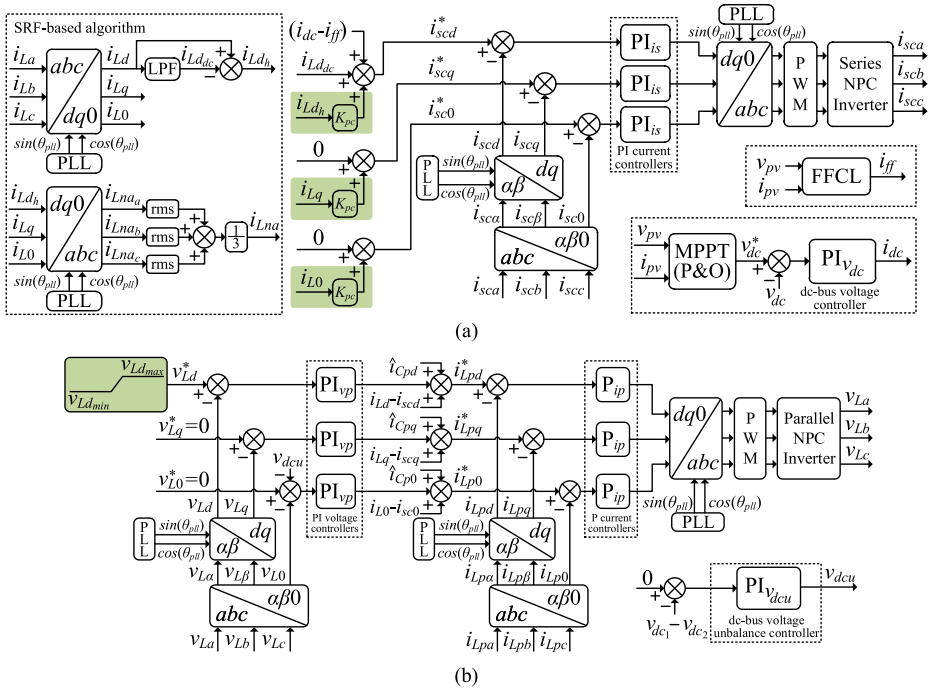

Fig. 4. Signal flow graphs of the control loops of the series and parallel NPC inverters. (a) Series current control loop and reference current generation with power limitation capability of the parallel converter. (b) parallel output voltage control loop with power relieve capability of the series converter.

where I_{Lna} is the nonactive rms load current; I_{pc} is the specified rms parallel converter current, $I_{\rm pv}$ and $I_{B\rm dc}$ are, respectively, the rms currents corresponding to the active power generated by the PV array and consumed by dc bus; i_{ff} and $i_{\rm dc}$ are, respectively, the feed-forward and dc-bus currents [24]. As can be noted in (20), if $I_{Lna} < I_{Lna_{\max}}$, the constant $K_{pc} < 0$ (ideal condition).

In addition, the rms parallel inverter current is computed by

$$I_{pc} = \frac{S_{pc}}{V_L} = \frac{S_{pc}}{\frac{1}{\sqrt{3}} v^*_{Ld}} \tag{21}$$

where v^*_{Ld} is the input voltage reference of the parallel converter in the *d*-axis.

2) Power Optimization of the Series Converter Power Flow: An important issue to be addressed refers to the amplitude differences between the input and output PV-UPQC voltages. It must be highlighted that the higher the differences, the higher amount of power will flow through the series converter.

In order to overcome this undesired condition and reduce the power processed by the series NPC inverter, the amplitude of the parallel NPC inverter (output voltages), which is defined by the voltage reference v^*_{Ld}, must be automatically adjusted (up or down). It is considered that this adjustment must occur within a specified range defined by the designer and must follow the amplitude variations of the grid voltages.

Fig. 4(b) shows the control loop of the parallel NPC inverter in which the proposed voltage reference generation strategy is presented. As can be noted in the shaded area shown in Fig. 4(b), the magnitude of v^*_{Ld} can be changed between the voltage range ($v^*_{Ld_{\max}}$ and $v^*_{Ld_{\min}}$). In this paper, the voltage range of $\pm 5\%$ around the nominal rms value of the fundamental grid voltage (V_{s1n}) is adopted. It means that the output voltages will also vary $\pm 5\%$ around their nominal ones. Thus, the parallel NPC inverter voltage reference v^*_{Ld} can be calculated by

$$v^*_{Ld} = \frac{\sqrt{3}}{2}\left(V_{s1} + V_{s1n}\right) \tag{22}$$

where V_{s1} is the rms value of the fundamental utility voltage and $V_{s1n} = 127$ V (nominal rms output voltages).

IV. Stability Analysis of the PV-UPQC System

In this section, the stability analysis of the PV-UPQC system is presented, in order to analyze the ability of the series and parallel converters to remain stable even under occurrence of disturbances in both the load currents and grid voltages.

A. Stability Analysis for Load Variations

The analysis of series NPC inverter stability upon load variations in the PV-UPQC system can be performed by means of the closed-loop transfer function (TF) [24] given by

$$\frac{i_{sc\_dq0}(s)}{i^*_{sc\_dq0}(s)} = \frac{W\left(K_{Pis}s + K_{Iis}\right)}{L_{\rm eq\_sc}s^2 + \left(WK_{Pis} + R_{\rm eq\_sc}\right)s + WK_{Iis}} \tag{23}$$

where $W = K_{\rm pwm}(V_{\rm dc}/2)$, $L_{eq\_sc} = L_{sc} + L_{Tsc}$, and $R_{eq\_sc} = R_{Lsc} + R_{Tsc}$, where L_{Tsc} and R_{Tsc} are the leakage inductance and the series resistance of the coupling transformer, respectively; K_{Pis} and K_{Iis} are the proportional and integral controller gains used in the respective control loop, while K_{pwm} is the static gain of the NPC inverter.

According to the Routh–Hurwitz stability criterion and considering the polynomial of second order in the denominator of (23), it is verified that the necessary and sufficient condition to

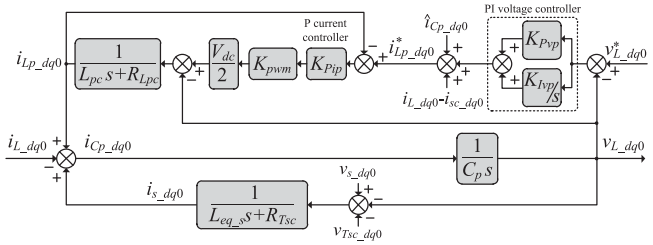

Fig. 5. Block diagram of the equivalent model adopted in the analysis of parallel converter stability for load variations.

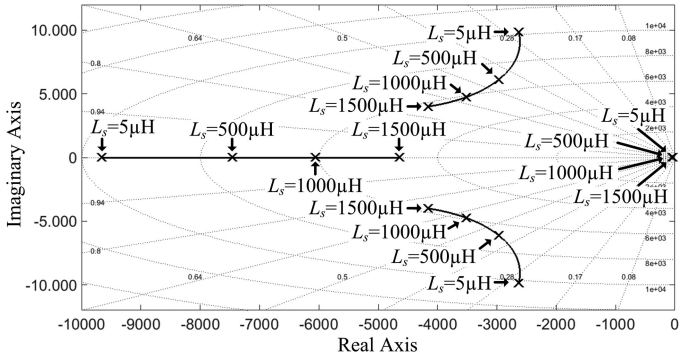

Fig. 6. Map of poles of the closed-loop TF adopted in the analysis of the parallel converter stability (5 μH $\leq$ L_s $\leq$ 1500 μH).

guarantee the system stability is that all the coefficients of the polynomial analyzed have the same signal. As shown in (23), all the coefficients are positive, meaning that the system is always stable. In this case, since this converter operates as a sinusoidal current source, load variations influence only the amplitude of the current reference of its control loop, without affecting the stability of the system.

The control loop of the parallel NPC inverter voltages can be represented in the SRF *dq*0-axes by the block diagram shown in Fig. 5, which considers load current (i_L) as the system input and the load voltage (v_L) as the system output. In order to perform the proper representation of this system, the grid currents i_s are obtained taking into account the grid inductances L_s, the series transformer leakage inductances L_{Tsc}, such that the equivalent inductances are given by $L_{\text{eq\_}s} = L_s + L_{Tsc}$, and the series transformer resistances R_{Tsc}. Load (v_L), grid (v_s), and series transformer (v_{Tsc}) voltages are also shown in Fig. 5.

From the block diagram in Fig. 5, it is possible to obtain the following closed-loop TF:

$$G_{v_L/i_L}(s) = \frac{v_{L\_dq0}(s)}{i_{L\_dq0}(s)} = \frac{X_1 s^3 + X_2 s^2 + X_3 s}{Y_1 s^4 + Y_2 s^3 + Y_3 s^2 + Y_4 s + Y_5} \tag{24}$$

where

$$\begin{aligned}
&X_1 = -L_{pc}L_{\text{eq_}s};\ X_2 = -L_{pc}R_{Tsc} - R_{Lpc}L_{\text{eq_}s} - L_{\text{eq_}s}K;\\
&X_3 = -R_{Lpc}R_{Tsc} - R_{Tsc}K;\\
&Y_1 = C_p L_{pc} L_{\text{eq_}s};\ Y_2 = C_p L_{pc} R_{Tsc} + C_p R_{Lpc} L_{\text{eq_}s}\\
&\quad + C_p L_{eq_s} K;\ Y_3 = C_p R_{Lpc} R_{Tsc} + K_{Pvp} L_{\text{eq_}s} K\\
&\quad + L_{\text{eq_}s} + L_{pc} + C_p R_{Tsc} K;\ Y_4 = K_{Pvp} R_{Tsc} K\\
&\quad + K_{Ivp} L_{eq_s} K + R_{Tsc} + R_{Lpc} + K;\\
&Y_5 = K_{Ivp} R_{Tsc} K;\ K = K_{Pip} K_{\text{pwm}} (V_{\text{dc}}/2).
\end{aligned}$$

whereby K_{Pvp}, K_{Ivp}, and K_{Pip} are the respective gains of the PI and P controllers used in the current control loop (inner loop) and voltage control loop (outer loop) of the parallel converter.

By means of the Routh–Hurwitz stability criterion and considering the polynomial of fourth order in the denominator of (24), some conditions must be met to ensure the system stability, as follows: 1) all coefficients of the polynomial denominator must have the same signal; and 2) the inequalities $Y_2Y_3 > Y_1Y_4$ and $Y_3 > (Y_2Y_5/Y_4) + (Y_1Y_4/Y_2)$ must be fulfilled. As can be seen in (24), all the coefficients of the mentioned polynomial are positive, which ensures that the first condition is always met. On the other hand, condition two can be met through proper adjustment of the controller gains K_{Pvp}, K_{Ivp}, and K_{Pip}. Therefore, it can be concluded that the system will be always stable, even when load transients occur.

Fig. 6 shows the TF poles of $G_{v_L/i_L}(s)$ for different values of L_s, where it turns out that all poles of a TF are in the left half-plane of the s-plane. This shows that different grid impedance characteristics do not affect the system stability.

B. Stability Analysis for Grid Voltage Variations

In conditions of grid voltage disturbances, the system stability analysis can be performed by means of the closed-loop TF involving the output voltages of the parallel NPC inverter, as given by

$$\frac{v_{L\_dq0}(s)}{v^*_{L\_dq0}(s)} = \frac{X_1 s + X_2}{Y_1 s^3 + Y_2 s^2 + Y_3 s + Y_4} \tag{25}$$

where

$$\begin{aligned}
&X_1 = K_{Pvp} K_{Pip} K_{\text{pwm}} (V_{\text{dc}}/2);\\
&X_2 = K_{Ivp} K_{Pip} K_{\text{pwm}} (V_{\text{dc}}/2);\\
&Y_1 = L_{pc} C_p;\ Y_2 = [R_{Lpc} + K_{Pip} K_{\text{pwm}} (V_{\text{dc}}/2)] C_p;\\
&Y_3 = K_{Pvp} K_{Pip} K_{\text{pwm}} (V_{\text{dc}}/2) + 1;\\
&Y_4 = K_{Ivp} K_{Pip} K_{\text{pwm}} (V_{\text{dc}}/2).
\end{aligned}$$

By applying the Routh–Hurwitz stability criterion and considering the polynomial of third order in the denominator of (25), the system is stable only if all coefficients in the mentioned polynomial have the same signal and the inequality $Y_2Y_3 > Y_1Y_4$ is met. It can be noted that the system stability is guaranteed through appropriate adjustments of the controller gains K_{Pvp}, K_{Ivp}, and K_{Pip}. Thus, variations in the grid voltage do not impact the system stability, since the dual compensation strategy is adopted, and the parallel inverter always feed the loads with sinusoidal, balanced, and regulated voltages. On the other hand, the differences between the input voltages v_s and output voltages v_L can be characterized as disturbances for the current control loop of the series NPC inverter. This control loop can be represented in the SRF *dq*0-axes, as shown in Fig. 7, which

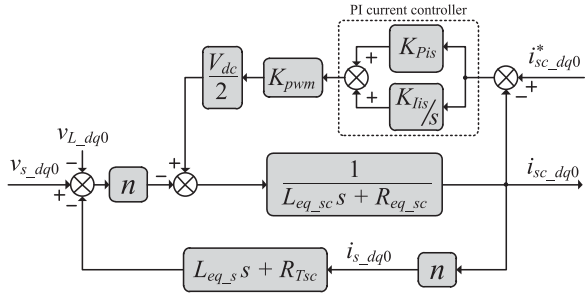

Fig. 7. Block diagram of the equivalent model adopted for the analysis of series inverter stability.

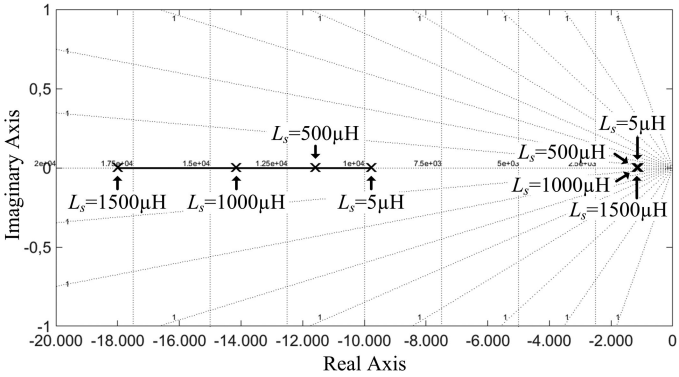

Fig. 8. Map of poles of the closed-loop TF adopted in the analysis of the series converter stability (5 μH $\leq L_s \leq$ 1500 μH).

relates the output currents of the series converter (i_{sc_dq0}) as a function of the grid voltages (v_{s_dq0}). Thus, from the block diagram shown in Fig. 7, the following closed-loop TF can be obtained:

$$G_{i_{sc}/v_s}(s) = \frac{i_{sc\_dq0}(s)}{v_{s\_dq0}(s)} = \frac{-ns}{\left(L_{\mathrm{eq}\_sc} - L_{\mathrm{eq}\_s}n^2\right)s^2 + \left(R_{\mathrm{eq}\_sc} + K_{Pis}W - R_{Tsc}n^2\right)s + K_{Iis}W} \quad (26)$$

where n is the transformation ratio of the series transformer.

Using the Routh–Hurwitz stability criterion and considering the polynomial of third order in the denominator in (26), the system stability is only ensured if all the coefficients in the polynomial denominator have the same signal. In this case, this condition is always met once $L_{\mathrm{eq}\_sc} > L_{\mathrm{eq}\_s}n^2$ or $R_{\mathrm{eq}\_sc} + K_{Pis}W > R_{Tsc}n^2$. Thus, even in the occurrence of grid voltage disturbances, the system stability is always achieved.

Fig. 8 shows the TF poles of $G_{i_{sc}/v_s}(s)$ for different values of L_s, where it turns out that different grid impedance characteristics do not affect the system stability.

V. Simulation Results

In this section, the proposed strategy developed to avoid the over power rating of the parallel NPC inverter is tested by means of numerical simulation using the MATLAB/Simulink tool. In such tests, it is defined that the parallel converter is sized to process a maximum apparent power $S_{pc_{\max}} = 3$ kVA. Figs. 9 and 10 present the waveforms of the grid voltages (v_{s_abc}), the grid currents (i_{s_abc}), the load voltages (v_{L_abc}), the load currents (i_{L_abc}), and the parallel converter currents (i_{pc_abc}). In addition, the total apparent powers of the grid (S_s) and parallel converter (S_{pc}) are also shown, considering the maximum power reference ($S_{pc_{\max}}$), and the power attenuation constant (K_{pc}), for the PV-UPQC system operating in OPM 3 ($P_{\mathrm{pv}} \cong 2.9$ kW). The nonlinear load employed is a three-phase full-bridge rectifier followed by *RC* load with apparent power $S_L \cong 2.4$ kVA ($R = 60\ \Omega$ and $C = 235\ \mu$F).

Fig. 9 presents the results related to the PV-UPQC operating without applying any power limitation to the parallel converter, such that $K_{pc} = 0$ (the over power rating strategy is inhibited). As can be noted in Fig. 9(a) and (b), the parallel converter processes both the active power, which is provided by the PV array, and compensate all the nonactive power demanded by the load (realize that the compensated grid currents are sinusoidal and in opposite phase with the respective grid voltages). In this case, it can be noted that the over power rating of the parallel converter occurs, as shown in Fig. 9(c). On the other hand, when the power limitation strategy is used in conjunction with the current control loop of the series converter, the apparent power processed by the parallel converter is properly adjusted ($K_{pc} \cong 0.4$), as shown in Fig. 10. As expected, part of the nonfundamental components of the load currents is now drained from the grid. It can be realized that the compensated grid currents are nonsinusoidal; however, they are still in opposite phase in relation to their respective grid voltages, meaning that the active power produced by the PV array remains being injected into the grid.

VI. Experimental Results

Experiments in this work were conducted by means of a prototype based on the scheme shown in Fig. 1. The parameters and the three-phase nonlinear load adopted in the experiments are presented in Table III. In both NPC inverters, the sinusoidal pulsewidth modulation technique was adopted [31].

Figs. 11–13 present the results obtained for the PV-UPQC system operating in OPM 1, 2, and 3 described in Section II-B. The rms values of voltages and currents are shown, as follows: grid (V_{s_abc}, I_{s_abc}); load (V_{L_abc}, I_{L_abc}); series NPC inverters (V_{Tsc_abc}, I_{s_abc}); and parallel NPC inverters (V_{L_abc}, I_{pc_abc}). Their respective apparent powers (S_{s_abc}, S_{L_abc}, S_{sc_abc}, S_{pc_abc}) and active powers (P_{s_abc}, P_{L_abc}, P_{sc_abc}, P_{pc_abc}), as well as the values of voltage, current, apparent power, and active power of the PV array (V_{pv}, I_{pv}, S_{pv}, P_{pv}), are also presented. In addition, the waveforms of the grid voltages (v_{s_abc}), load voltages (v_{L_abc}), series transformer voltages (v_{Tsc_abc}), grid currents (i_{s_abc}), load currents (i_{L_abc}), and parallel converter currents (i_{pc_abc}), as well as the voltage and current of the PV array (v_{pv}, i_{pv}), are shown. These measurements were carried out using the YOKOGAWA WT3000 power analyzer.

The results shown in Fig. 11 were obtained with the PV-UPQC system operating as the UPQC (OPM 2), that is, with $P_{pv} = 0$ W, whereas $V_s < V_L$. In Fig. 11(a)–(c), the rms values of voltage and current are shown along with their active and apparent powers. As expected for this OPM, it is observed that

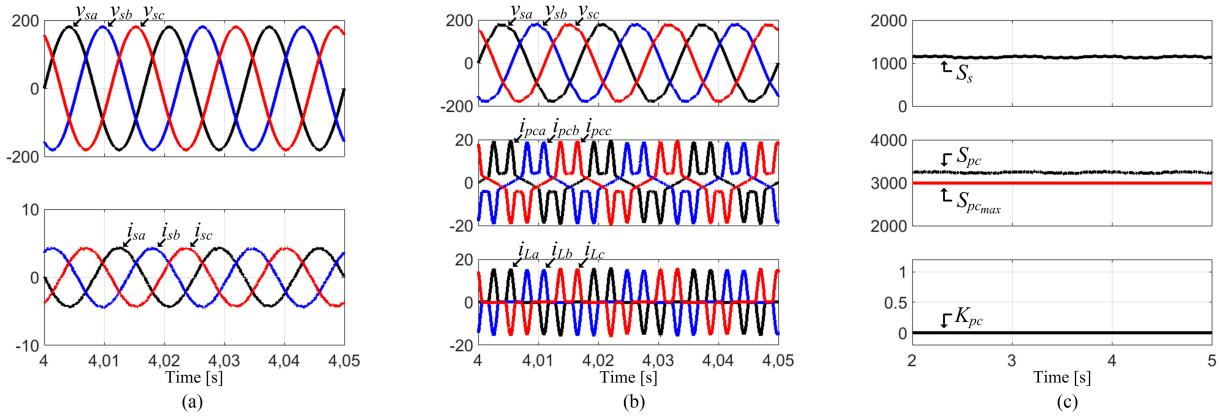

Fig. 9. OPM 3: PV-UPQC performing active power injection and active power filtering without the power limitation algorithm of the parallel NPC inverter (P_{pv} ≅ 2900 W). (a) Grid voltages (v_{s_abc}) and grid currents (i_{s_abc}). (b) Load voltages (v_{L_abc}), parallel converter currents (i_{pc_abc}), and load currents (i_{L_abc}). (c) Total apparent power of the grid (S_s), total apparent power of the parallel converter (S_{pc}) and power limit reference ($S_{pc_{\max}}$), and power attenuation constant (K_{pc}).

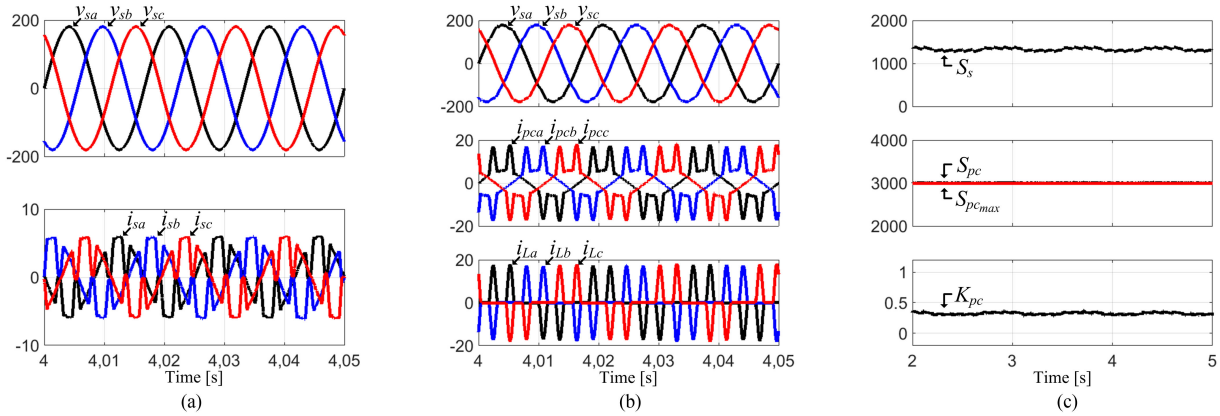

Fig. 10. OPM 3: PV-UPQC performing active power injection and active power filtering with the power limitation algorithm of the parallel NPC inverter (P_{pv} ≅ 2900 W). (a) Grid voltages (v_{s_abc}) and grid currents (i_{s_abc}). (b) Load voltages (v_{L_abc}), parallel converter currents (i_{pc_abc}), and load currents (i_{L_abc}). (c) Total apparent power of the grid (S_s), total apparent power of the parallel converter (S_{pc}) and power limit reference ($S_{pc_{\max}}$), and power attenuation constant (K_{pc}).

TABLE III
PARAMETERS ADOPTED IN THE EXPERIMENTS

Nominal rms grid voltages		V_s = 127.27 V
Utility grid frequency		f_s = 60 Hz
Inductive filters (series NPC inverter)		L_{sc} = 3.5 mH
Internal resistances of the series NPC inverter inductors		R_{Lsc} = 0.2 Ω
Leakage inductance of series coupling transformers		L_{Tsc} = 0.12 mH
Resistances of series coupling transformers		R_{Tsc} = 0.28 Ω
Inductive Filters (parallel NPC inverter)		L_{pc} = 1.73 mH
Internal resistances of the parallel NPC inverter inductors		R_{Lpc} = 0.2 Ω
Capacitive filters (parallel NPC inverter)		C_p = 60 µF
dc-bus equivalent capacitance		C_{dc} = 2350 µF
dc-bus voltage (MPP in STC)		V_{dc} = 616 V
Minimum dc-bus voltage		v^*_{dc} = 460 V
NPC inverter switching frequency		f_{sw} = 20 kHz
A/D converter sampling frequency		f_{ad} = 60 kHz
P&O-MPPT sampling frequency		$f_{P\&O}$ = 10 Hz
P&O-MPPT voltage increment step		Δv = 1V
PWM gain		K_{pwm} = 0.0002
Load - Three-phase full-wave rectifier with resistive load (R = 40 Ω)		
S_{La} = 782.92 W	S_{Lb} = 777.93 W	S_{Lc} = 783.92 VA
P_{La} = 747.54 VA	P_{Lb} = 741.79 VA	P_{Lc} = 749.80 VA

part of the active power drained from the grid flows through the series and parallel converters of the UPQC. It is also observed that there is some flow of active power ($P_{B\mathrm{dc}}$) from the grid to the dc bus via a parallel converter, to compensate losses in the system involving the passive elements and the power switches of the NPC inverters. Fig. 11(d)–(f) shows the voltage and current waveforms. As can be noted, the parallel converter fed the load with regulated, balanced, and sinusoidal voltages. Moreover, the difference between input and output voltages appears across the terminals of the series coupling transformers. Finally, it is observed that the grid currents are sinusoidal and are in phase with their respective voltages, that is, the harmonic components of the load currents flow through the parallel converter rather than through the grid.

In Fig. 12, the results of the PV-UPQC system operating in OPM 3 ($P_{pv} > P_L$ and $V_s \cong V_L$) are shown, that is, in addition to active series and parallel power-line conditioning, the PV system injects active power into the grid. It can be seen, in Fig. 12(a)–(c), that the power processed in each of the legs of the parallel converter is approximately 30% of the active power

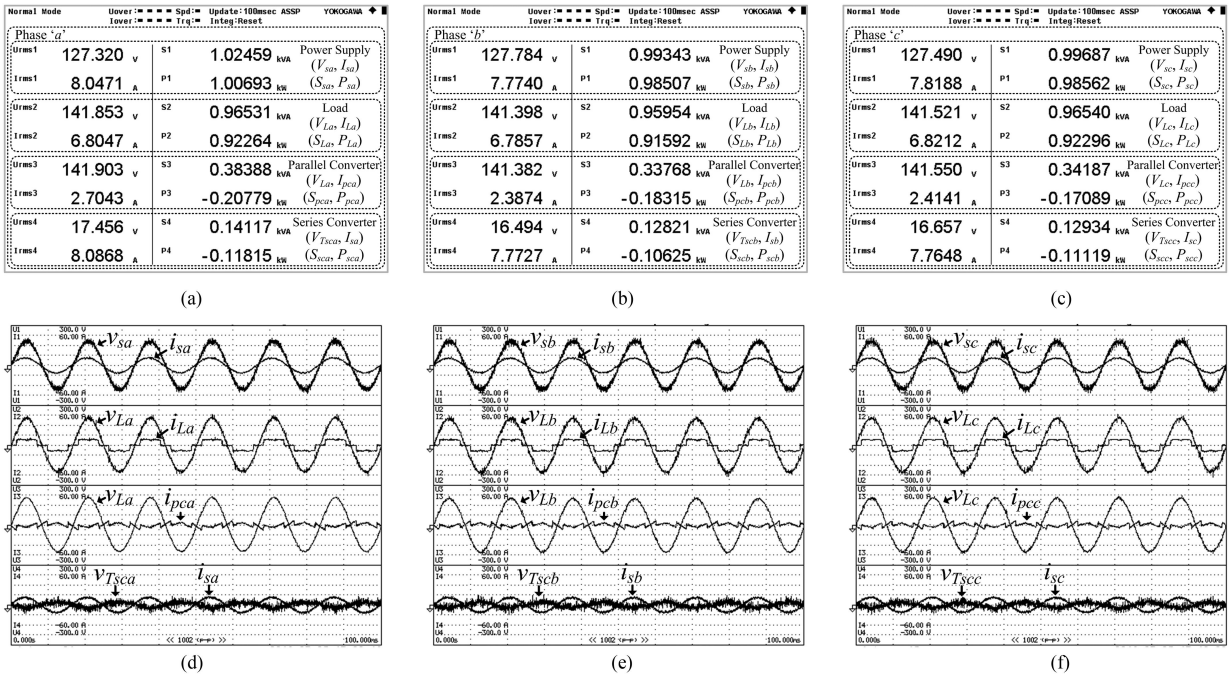

Fig. 11. OPM 2: PV-UPQC performing only active power-line conditioning ($P_{pv} = 0$ W and $V_s < V_L$). (a) Magnitudes of the phase "*a*." (b) Magnitudes of the phase "*b*." (c) Magnitudes of the phase "*c*." (d) Waveforms of voltage and current of the phase "*a*." (e) Waveforms of voltage and current of the phase "*b*." (f) Waveforms of voltage and current of the phase "*c*."

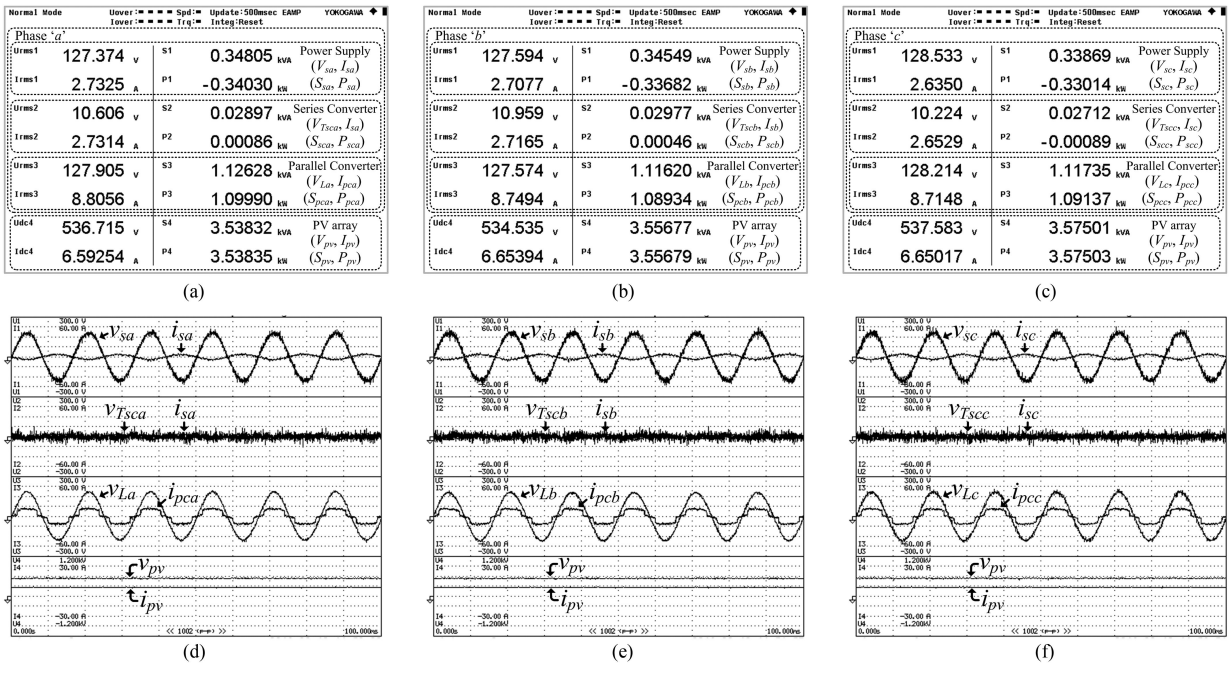

Fig. 12. OPM 3: PV-UPQC performing active power injection and active power-line conditioning ($P_{pv} > P_L$ and $V_s \cong V_L$). (a) Magnitudes of the phase "*a*." (b) Magnitudes of the phase "*b*." (c) Magnitudes of the phase "*c*." (d) Waveforms of voltage and current of the phase "*a*." (e) Waveforms of voltage and current of the phase "*b*." (f) Waveforms of voltage and current of the phase "*c*."

drained from the PV array. Part of this power is consumed by the load ($P_{L\_abc} \cong 750$ W) and the remaining is injected into the grid. It can be also noted that, as $V_s \cong V_L$, the flow of active power through the series converter is very small. Fig. 12(d)–(f) shows the voltage and current waveforms. It appears that the load is fed by the PV-UPQC system via a parallel converter, and that the series inverter remains synthesizing sinusoidal and balanced grid currents, but in phase opposition with their respective grid voltages.

The results obtained for the PV-UPQC system operating in OPM 1, that is, only performing the injection of active power into the grid ($P_{L\_abc} = 0$ W, $V_s \cong V_L$), are shown in

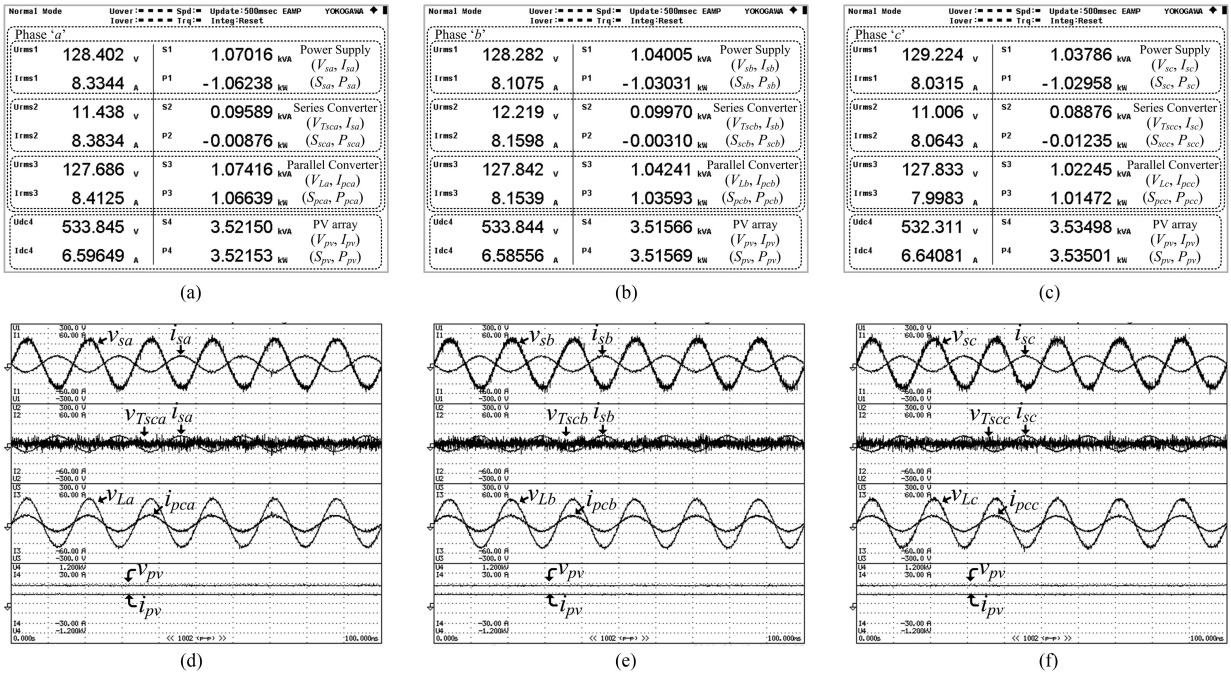

Fig. 13. OPM 1: PV-UPQC performing only active power injection into the grid ($P_{\rm L} = 0$ W and $V_s \cong V_L$). (a) Magnitudes of the phase "*a*." (b) Magnitudes of the phase "*b*." (c) Magnitudes of the phase "*c*." (d) Waveforms of voltage and current of the phase "*a*." (e) Waveforms of voltage and current of the phase "*b*." (f) Waveforms of voltage and current of the phase "*c*."

TABLE IV
MAGNITUDES MEASURED IN THE PV-UPQC SYSTEM

Phases	THD_{V_s}	THD_{i_L}	PF_{1L}	V_s/V_L	K_{Bdc}	k_{pv}	$\lvert S_L\rvert$(VA)	$\lvert S_{sc}\rvert$(VA)	$\lvert S_{sc}\rvert/\lvert S_L\rvert$ (real)	$\lvert S_{sc}\rvert/\lvert S_L\rvert$ (ideal)	$\lvert S_{pc}\rvert$(VA)	$\lvert S_{pc}\rvert/\lvert S_L\rvert$ (real)	$\lvert S_{pc}\rvert/\lvert S_L\rvert$ (ideal)
OPM 2													
'a'	1.8%	27%	1	0.89	0.082	0	965.31	141.17	0.146	0.130	383.88	0.397	0.334
'b'	1.8%	27%	1	0.90	0.082	0	959.54	128.21	0.133	0.118	337.68	0.351	0.326
'c'	1.8%	27%	1	0.90	0.082	0	965.40	129.34	0.133	0.118	341.87	0.354	0.326
OPM 3													
'a'	1.8%	27%	1	0.99	0.122	1.58	782.92	28.97	0.037	0.009	1126.28	1.438	1.436
'b'	1.8%	27%	1	1.00	0.122	1.58	777.93	29.77	0.038	0.007	1116.20	1.434	1.432
'c'	1.8%	27%	1	1.00	0.122	1.58	783.92	27.12	0.034	0.007	1117.35	1.425	1.432

Fig. 13. It is observed that, as $V_s \cong V_L$, the parallel converter processes almost all the active power injected into the grid. It is also observed that the grid currents are sinusoidal, balanced, and in phase opposition with their respective grid voltages.

In both cases shown in Figs. 12 and 13, approximately 9% of the active power drained from the PV array is consumed by the PV-UPQC system to compensate the losses related to switching and filtering passive elements.

Table IV summarizes the results measured for the PV-UPQC system operating in OPM 2 and 3. It is noted that all the measured values are in accordance with the power flow study presented in Section III.

Fig. 14 shows some results of the PV-UPQC system operating in OPM 3 and grid-islanded mode (OPM 4). The dc-bus voltages ($v_{\rm dc}$, $v_{\rm dc1}$, $v_{\rm dc2}$), grid current (i_{sa}), and load voltage and current (v_{La} and i_{La}) are presented. In Fig. 14(a), the PV-UPQC system operates in OPM 3, whereby $P_{pv} > P_L$, while in Fig. 14(b), the system operates in OPM 4. In this case, the series converter is turned OFF (inhibited), while the parallel converter remains turned ON feeding the load with the power produced from the PV array. Fig. 14(c) shows the behavior of the system for the transitions from OPM 3 to OPM 4 and vice versa. An increase in the dc-bus voltage ($v_{\rm dc}$) during the grid-islanded operation mode can be seen, because the MPPT algorithm is disabled. In this case, the dc-bus voltage level goes to a specific operation point, which depends on the amount of energy that is being drained from the PV array. Fig. 14(d) and (e) shows the quantities i_{sa}, v_{La}, and i_{La} when the transitions occur. It can be noted that, if there is enough power in the dc bus, there is no interruption of the power supplied to the load. In addition, these transitions do not affect the parallel converter output voltages (load voltages). Finally, Fig. 14(f) shows dc-bus voltages ($v_{\rm dc}$, $v_{\rm dc1}$, $v_{\rm dc2}$) and the grid current in the phase "a" (i_{sa}). It can be observed that $v_{\rm dc1}$ and $v_{\rm dc2}$ remain balanced even when the system operates in the grid-islanded mode, since the control loop of the unbalance of dc-bus voltages is implemented in conjunction with the control loop of the output voltages.

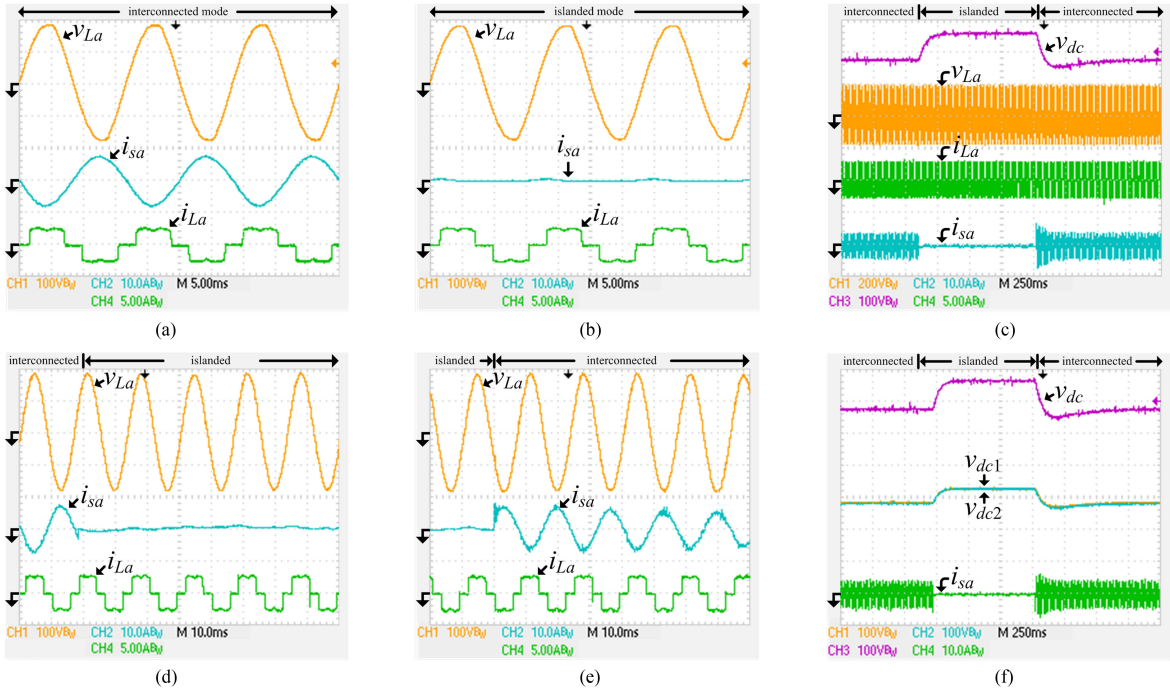

Fig. 14. Experimental results involving v_{La} voltage (100 V/div), i_{sa} (10 A/div) and i_{La} (5 A/div) currents, and $v_{\rm dc}$, $v_{\rm dc1}$, and $v_{\rm dc2}$ voltages (100 V/div) for transitions between grid-connected and grid-islanded modes (OPM 3 and OPM 4), with $P_{pv} > P_L$. (a) Grid-connected mode (5 ms/div). (b) Islanded mode (5 ms/div). (c) Transition from the grid-connected to grid-islanded mode and vice versa (250 ms/div). (d) Transition from grid-connected to grid-islanded mode (10 ms/div). (e) Transition from grid-islanded to grid-connected mode (10 ms/div). (f) Dynamic behavior of $v_{\rm dc}$, $v_{\rm dc1}$, and $v_{\rm dc2}$ during the transitions (250 ms/div).

VII. Conclusion

This paper presented detailed studies involving the power flow and stability analysis of a multifunctional PV-DG system integrated with a UPQC, which was entirely based on the adopted dual compensation strategy and distinct operation modes.

With respect to the study of the power flow, several mathematical equations and extensive normalized curves involving the apparent power of both series and parallel converters were presented, as well as detailed analyses of the active power flowing through the PV-UPQC system. This study emerges as an important methodology for properly sizing the power converters, taking into account not only the influence of some existing disturbances in the grid voltages, as well as the nonlinear characteristics of the load, but also the maximum power generated by the PV array. Furthermore, two strategies aimed at limiting and/or decreasing the power rating of the UPQC inverters were presented and discussed.

For the system stability analysis, the variations in both load currents and grid voltages were considered as disturbances. Such analysis showed that, with the adopted voltage and current controllers, the system stability is always ensured, even for distinct grid impedance characteristics.

Besides simulation results, which showed the effectiveness to overcome the over power rating of the parallel converter, experimental results were presented considering different static conditions of operation of the PV-UPQC system. Thus, it was possible to quantitatively validate the study involving the power flows. In addition, the dynamic behavior of the system was evaluated under transition conditions from grid-connected mode to grid-islanded mode, and vice versa, where no voltage transients in the load were observed. These results showed that, even in the absence of the utility grid, the PV-UPQC system can continue processing the energy generated by the PV array, which highlights the multifunctionality of the system in applications involving ac microgrids.

References

[1] J. M. Guerrero *et al.*, "Distributed generation: Toward a new energy paradigm," *IEEE Ind. Electron. Mag.*, vol. 4, no. 1, pp. 52–64, Mar. 2010.

[2] M. H. Nehrir *et al.*, "A review of hybrid renewable/alternative energy systems for electric power generation: Configurations, control, and applications," *IEEE Trans. Sustain. Energy*, vol. 2, no. 4, pp. 392–403, Oct. 2011.

[3] S. Bacha, D. Picault, B. Burger, I. Etxeberria-Otadui, and J. Martins, "Photovoltaics in microgrids: An overview of grid integration and energy management aspects," *IEEE Ind. Electron. Mag.*, vol. 9, no. 1, pp. 33–46, Mar. 2015.

[4] S. B. Kjaer, J. K. Pedersen, and F. Blaabjerg, "A review of single-phase grid-connected inverters for photovoltaic modules," *IEEE Trans. Ind. Appl.*, vol. 41, no. 5, pp. 1292–1306, Sep./Oct. 2005.

[5] W. Li, Y. Gu, H. Luo, W. Cui, X. He, and C. Xia, "Topology review and derivation methodology of single-phase transformerless photovoltaic inverters for leakage current suppression," *IEEE Trans. Ind. Electron.*, vol. 62, no. 7, pp. 4537–4551, Jul. 2015.

[6] L. Zhang, K. Sun, L. Feng, H. Wu, and Y. Xing, "A family of neutral point clamped full-bridge topologies for transformerless photovoltaic grid-tied inverters," *IEEE Trans. Power Electron.*, vol. 28, no. 2, pp. 730–739, Feb. 2013.

[7] F. A. S. Neves, M. Carrasco, F. Mancilla-David, G. M. S. Azevedo, and V. S. Santos, "Unbalanced grid fault ride-through control for single-stage photovoltaic inverters," *IEEE Trans. Power Electron.*, vol. 31, no. 4, pp. 3338–3347, Apr. 2016.

[8] H. Xiao and S. Xie, "Transformerless split-inductor neutral point clamped three-level PV grid-connected inverter," *IEEE Trans. Power Electron.*, vol. 27, no. 4, pp. 1799–1808, Apr. 2012.

[9] W. Libo, Z. Zhengming, and L. Jianzheng, "A single-stage three-phase grid-connected photovoltaic system with modified MPPT method and reactive power compensation," *IEEE Trans. Energy Convers.*, vol. 22, no. 4, pp. 881–886, Dec. 2007.
[10] M. C. Cavalcanti, A. M. Farias, K. C. Oliveira, F. A. S. Neves, and J. L. Afonso, "Eliminating leakage currents in neutral point clamped inverters for photovoltaic systems," *IEEE Trans. Ind. Electron.*, vol. 59, no. 1, pp. 435–443, Jan. 2012.
[11] Y. Tang, W. Yao, P. C. Loh, and F. Blaabjerg, "Highly reliable transformerless photovoltaic inverters with leakage current and pulsating power elimination," *IEEE Trans. Ind. Electron.*, vol. 63, no. 2, pp. 1016–1026, Feb. 2016.
[12] Y. Kim, H. Cha, B. M. Song, and K. Y. Lee, "Design and control of a grid-connected three-phase 3-level NPC inverter for building integrated photovoltaic systems," in *Proc. IEEE PES Innov. Smart Grid Technol.*, 2012, pp. 1–7.
[13] G. Ding *et al.*, "Adaptive dc-link voltage control of two-stage photovoltaic inverter during low voltage ride-through operation," *IEEE Trans. Power Electron.*, vol. 31, no. 6, pp. 4182–4194, Jun. 2016.
[14] S. A. O. Silva, L. P. Sampaio, F. M. Oliveira, and F. R. Durand, "Feed-forward dc-bus control loop applied to a single-phase grid-connected PV system operating with PSO-based MPPT technique and active power-line conditioning," *IET Renew. Power Gener.*, vol. 11, no. 1, pp. 183–193, Jan. 2017.
[15] T. Wu, H. Nien, C. Shen, and T. Chen, "A single-phase inverter system for PV power injection and active power filtering with nonlinear inductor consideration," *IEEE Trans. Ind. Appl.*, vol. 41, no. 4, pp. 1075–1083, Jul./Aug. 2005.
[16] S. Sezen, A. Aktas, M. Ucar, and E. Ozdemir, "Design and operation of a multifunction photovoltaic power system with shunt active filtering using a single-stage three-phase multilevel inverter," *Turkish J. Electr. Eng. Comput. Sci.*, vol. 25, pp. 1412–1425, Apr. 2017.
[17] L. B. G. Campanhol, S. A. O. Silva, A. A. O. Júnior, and V. D. Bacon, "Dynamic performance improvement of a grid-tied PV system using a feed-forward control loop acting on the NPC inverter currents," *IEEE Trans. Ind. Electron.*, vol. 64, no. 3, pp. 2092–2101, Mar. 2017.
[18] J. M. Guerrero, P. C. Loh, T. Lee, and M. Chandorkar, "Advanced control architectures for intelligent microgrids—Part II: Power quality, energy storage, and ac/dc microgrids," *IEEE Trans. Ind. Electron.*, vol. 60, no. 4, pp. 1263–1270, Apr. 2013.
[19] J. Rocabert, A. Luna, F. Blaabjerg, and P. Rodríguez, "Control of power converters in ac microgrids," *IEEE Trans. Power Electron.*, vol. 27, no. 11, pp. 4734–4749, Nov. 2012.
[20] IEEE Standard Definitions for the Measurement of Electric Power Quantities Under Sinusoidal, Nonsinusoidal, Balanced, or Unbalanced Conditions, IEEE Std. 1459-2010, Mar. 2010.
[21] M. C. Cavalcanti, G. M. S. Azevedo, B. A. Amaral, and F. A. S. Neves, "Unified power quality conditioner in a grid connected photovoltaic system," *Electr. Power Qual. Utilization J.*, vol. XII, no. 2, pp. 59–69, 2006.
[22] S. Devassy and B. Singh, "Dynamic performance of solar PV integrated UPQC-P for critical loads," in *Proc. Annu. IEEE India Conf.*, 2015, pp. 1–6.
[23] B. Han, B. Bae, H. Kim, and S. Baek, "Combined operation of unified power-quality conditioner with distributed generation," *IEEE Trans. Power Del.*, vol. 21, no. 1, pp. 330–338, Jan. 2006.
[24] L. B. G. Campanhol, S. A. O. Silva, A. A. Oliveira Jr., and V. D. Bacon, "Single-stage three-phase grid-tied PV system with universal filtering capability applied to DG systems and ac microgrids," *IEEE Trans. Power Electron.*, vol. 32, no. 12, pp. 9131–9142, Dec. 2017.
[25] R. A. Modesto, S. A. O. Silva, and A. A. Oliveira Jr., "Power quality improvement using a dual unified power quality conditioner/ uninterruptible power supply in three-phase four-wire systems," *IET Power Electron.*, vol. 8, no. 9, pp. 1595–1605, Aug. 2015.
[26] R. A. Modesto, S. A. O. Silva, A. A. Oliveira Jr., and V. D. Bacon, "A versatile unified power quality conditioner applied to three-phase four-wire distribution systems using a dual control strategy," *IEEE Trans. Power Electron.*, vol. 31, no. 8, pp. 5503–5514, Aug. 2016.
[27] B. W. França, L. F. Silva, M. A. Aredes, and M. Aredes, "An improved iUPQC controller to provide additional grid-voltage regulation as a STATCOM," *IEEE Trans. Ind. Electron.*, vol. 62, no. 3, pp. 1345–1352, Mar. 2015.
[28] H. Fujita and H. Akagi, "The unified power quality conditioner: the integration of series and shunt-active filters," *IEEE Trans. Power Electron.*, vol. 13, no. 2, pp. 315–322, Mar. 1998.
[29] N. L. Díaz, J. C. Vasquez, and J. M. Guerrero, "A communication-less distributed control architecture for islanded microgrids with renewable generation and storage," *IEEE Trans. Power Electron.*, vol. 33, no. 3, pp. 1922–1939, Mar. 2018.
[30] V. D. Bacon and S. A. O. Silva, "Performance improvement of a three-phase phase-locked-loop algorithm under utility voltage disturbances using non-autonomous adaptive filters," *IET Power Electron.*, vol. 8, no. 11, pp. 2237–2250, Nov. 2015.
[31] I. Colak, E. Kabalci, and R. Bayindir, "Review of multilevel voltage source inverter topologies and control schemes," *Energy Convers. Manag.*, vol. 52, no. 2, pp. 1114–1128, 2011.

Leonardo Bruno Garcia Campanhol received the B.S. degree in industrial automation technology and the M.S. degree in electrical engineering from the Federal University of Technology, Cornélio Procópio, PR, Brazil, in 2009 and 2012, respectively, and the Ph.D. degree in electrical engineering from the São Carlos Engineering School, University of São Paulo, São Carlos, SP, Brazil, in 2017.

Since 2013, he has been with the Electrical Engineering Department, Federal University of Technology, Apucarana, PR, Brazil, where he is currently an Associate Professor of electrical engineering. His research interests include power electronics applications involving unified power quality conditioner systems, active power-line filters, photovoltaic systems, power quality, and digital signal processing and applications.

Dr. Campanhol is a member of the Brazilian Power Electronics Society.

Sérgio Augusto Oliveira da Silva (M'13) received the B.S. and M.S. degrees from the Federal University of Santa Catarina, Florianopolis, SC, Brazil, in 1987 and 1989, respectively, and the Ph.D. degree from the Federal University of Minas Gerais, Belo Horizonte, MG, Brazil, in 2001, all in electrical engineering.

Since 1993, he has been with the Electrical Engineering Department, Federal University of Technology, Cornélio Procópio, PR, Brazil, where he is currently a Professor of electrical engineering and the Coordinator of the Laboratory of Power Electronics, Power Quality and Renewable Energies. His research interests include power electronics applications involving UPS systems, active power-line filters, photovoltaic systems, control systems, and power quality.

Dr. da Silva is a member of the Brazilian Power Electronics Society.

Azauri Albano de Oliveira Jr. received the B.S and M.S. degrees from the São Carlos Engineering School (EESC), University of São Paulo (USP), São Carlos, SP, Brazil, in 1977 and 1984, respectively, and the Ph.D. degree from the Polytechnic School, USP, in 1991, all in electrical engineering.

Since 1978, he has been with the Electrical and Computing Engineering Department, EESC, USP, where he is currently a Professor of electrical engineering and the Coordinator of the Power Electronics and Control Laboratory. His research interests include power electronics, electric machinery drives, wireless power transfer, and engineering education.

Vinícius Dário Bacon received the B.S. and M.S. degrees in electrical engineering in 2013 and 2015, respectively, from the Federal University of Technology (UTFPR-CP), Cornélio Procópio, PR, Brazil, where he is currently working toward the Ph.D. degree.

Since 2016, he has been with the Electrical Engineering Department, UTFPR-CP, where he is currently an Adjunct Professor of electrical engineering. His current research interests include power quality, active power filters, renewable energies, and digital signal processing and applications.

Mr. Bacon is a member of the Brazilian Power Electronics Society.